Published in final edited form as:

Carbon N Y. 2017 May ; 116: 191–200. doi:10.1016/j.carbon.2017.01.097.

Impact of UV irradiation on multiwall carbon nanotubes in nanocomposites: formation of entangled surface layer and mechanisms of release resistance

Tinh Nguyen, **Elijah J. Petersen***, **Bastien Pellegrin**[1], **Justin M. Gorham**, **Thomas Lam**, **Minhua Zhao**[2], and **Lipiin Sung***

National Institute of Standards and Technology (NIST), Gaithersburg, Maryland 20899

Abstract

Multiwall carbon nanotubes (MWCNTs) are nanofillers used in consumer and structural polymeric products to enhance a variety of properties. Under weathering, the polymer matrix will degrade and the nanofillers may be released from the products potentially impacting ecological or human health. In this study, we investigated the degradation of a 0.72 % (by mass) MWCNT/amine-cured epoxy nanocomposite irradiated with high intensity ultraviolet (UV) light at various doses, the effects of UV exposure on the surface accumulation and potential release of MWCNTs, and possible mechanisms for the release resistance of the MWCNT surface layer formed on nanocomposites by UV irradiation. Irradiated samples were characterized for chemical degradation, mass loss, surface morphological changes, and MWCNT release using a variety of analytical techniques. Under 295 nm to 400 nm UV radiation up to a dose of 4865 MJ/m^2, the nanocomposite matrix underwent photodegradation, resulting in formation of a dense, entangled MWCNT network structure on the surface. However, no MWCNT release was detected, even at very high UV doses, suggesting that the MWCNT surface layer formed from UV irradiation of polymer nanocomposites resist release. Four possible release resistance mechanisms of the UV-induced MWCNT surface layer are presented and discussed.

1. Introduction

Nanocomposites, materials containing a nanofiller (defined as any particle with a characteristic dimension between 1 nm and 100 nm) incorporated into the matrix material (*e.g.,* polymer, ceramic), often have novel or enhanced properties as compared to the unmodified matrix material [1]. For nanocomposites incorporating multiwall carbon nanotubes (MWCNTs), these changes may include enhanced mechanical strength, flame

*Corresponding authors: lipiin@nist.gov; elijah.petersen@nist.gov.
[1]Current address: Steap Stailor, Rue Dr Schweitzer, 38180 SEYSSINS - FRANCE
[2]Current address: X-wave Innovations, Inc., Gaithersburg, MD 20878, United States

Disclaimer: *Certain commercial product or equipment is described in this paper in order to specify adequately the experimental procedure. In no case does such identification imply recommendation or endorsement by the National Institute of Standards and Technology, nor does it imply that it is necessarily the best available for the purpose.*

Supplementary Data

Supplementary data associated with this article can be found in the online version.

retardant capacities, or electrical properties [2, 3], advantages that have or may result in potential applications in aerospace [4], construction [5], and consumer products [6].

For widespread market adoption of nanocomposites, it is important to understand if the nanofillers might have any adverse impacts. This could occur if environmental stresses (e.g., biodegradation, ultraviolet (UV) light, and moisture) cause release of the nanofiller [6–18]. MWCNTs are one nanofiller of concern for potential environmental and/or human health effects due to its high aspect ratio [7, 19–24]. There have been a number of studies conducted to date on release of MWCNTs due to mechanical stresses (e.g., abrasion, sanding, polishing) [1, 23, 25–35], yet fewer on the fate and release caused by environmental stresses [14, 17, 23, 31, 32, 36]. Recent studies on the potential toxicological effects of materials released from MWCNT nanocomposites have not shown increased toxicity compared to particles released from the polymer matrix under the environmental conditions tested [14, 23, 32, 33]. While release of individual MWCNT from nanocomposites has been detected in a few studies after abrasion [23, 30, 33] or sanding [29], most studies have not found detectable MWCNT release by exposures to weathering environments [13, 25–28, 31, 32, 35]. In fact, numerous studies have shown MWCNT accumulation on the nanocomposite surface after exposures to UV radiation [14, 17, 28, 31, 32, 37], the most dominant weathering element known to cause severe degradation of polymeric materials used outdoors [38]. The factors that cause MWCNT agglomeration and network formation on the surface are not yet well understood. In a previous study at a high MWCNT loading (3.5 % mass fraction based on the polymer solid matrix; all percentages in this study refer to a mass percentage of MWCNTs in the composite materials), we have observed a strong photostabilization effect of the epoxy matrix by MWCNT and a measurable quantity of MWCNT accumulated on the nanocomposite surface after exposure to UV radiation [37]. The impacts of UV irradiation on nanocomposites containing much lower MWCNT loadings are not known. Further, the main focus of the previous work was to develop methodologies for characterizing surface chemistry changes of the nanocomposites resulting from UV exposure, without any attempts to measure MWCNTs released from the irradiated nanocomposite.

In this study, we have investigated, using a suite of analytical methods developed and applied in our previous publication [37], the dose-dependent effects of UV irradiation on the degradation, surface accumulation, and potential for nanofiller release from nanocomposites containing a one-fifth of the MWCNT loading than previously studied, namely a 0.72 % MWCNT epoxy nanocomposite sample compared to the previously tested 3.5 % MWCNT epoxy nanocomposite sample. The results of this and previous experiments will provide essential data to assess the role of MWCNT concentration on the impact of UV radiation on MWCNT surface accumulation and release potential from a polymer nanocomposite. These experiments were conducted via accelerated aging using intense UV radiation with the same spectral regime as the UV portion of natural sunlight (295 nm to 400 nm) at elevated temperature (50 °C) and humidity (75 % relative humidity) in the National Institute of Standards and Technology (NIST) SPHERE (Simulated Photodegradation *via* High Energy Radiant Exposure) [39]. Based on our experimental results, which showed severe degradation of the matrix and a substantial MWCNT surface accumulation at both MWCNT loading concentrations but without an apparent release after a very high UV dose (4865

MJ/m^2, i.e., 9-month exposure), we present four potential mechanisms to explain the strong release resistance of the MWCNT surface layer formed on nanocomposites by UV irradiation. However, additional mechanical and environmental stresses to the nanocomposite after UV irradiation could also potentially result in release during the use, disposal, or recycling of MWCNT nanocomposites [34, 35, 40].

2. Experimental Section

2.1. Materials and Sample Preparation

Epoxy nanocomposite films containing a 0.72 % mass fraction of MWCNTs were used in this study. The matrix was a stoichiometric mixture of a diglycidyl ether of bisphenol A (DGEBA) epoxy resin having an equivalent mass of 189 and a polyoxypropylenetriamine curing agent. The epoxy matrix was used without UV stabilizers or additives. MWCNT was a commercial 1 % mass fraction pre-dispersed product in the same epoxy resin. To better understand the starting material, the sizes of the MWCNT were investigated using scanning electron microscopy (SEM) after extraction from the epoxy resin using a toluene extraction procedure described previously [37]. The estimated average MWCNT diameter was 20.5 nm with a standard deviation of 4.0 nm (n=200), and the lengths predominately ranged between 200 nm and 2 μm; challenges associated with accurately obtaining a MWCNT length distribution have been previously described [41]. SEM micrographs and a histogram of the MWCNT diameters are provided in Figure S1.

Free-standing films of unfilled epoxy (neat) and 0.72 % MWCNT epoxy composite were fabricated (note that the 1% mass fraction MWCNT in the epoxy resin is reduced to 0.72 % mass fraction in the amine-cured epoxy). Neat epoxy and MWCNT epoxy nanocomposite films were prepared by adding appropriate amounts of amine curing agent directly to the epoxy resin or the MWCNT pre-dispersed epoxy resin, respectively, and stirring for 1 h with a magnetic stirrer. After degassing for 1 h at room temperature, the epoxy/amine/MWCNT mixture was drawn down on a polyethylene terephthalate sheet attached to a vacuum table using a bar applicator to produce free standing films having a thickness of approximately 150 μm (cross sectional analysis performed by laser scanning confocal microscopy). Reagent grade toluene (purity > 99.5 %) was used for all composite processing. All coated samples were cured at ambient conditions (24 °C and 45 % relative humidity) for three days, followed by post-curing at 110 °C for 4 h in an air circulating oven. The dispersion of MWCNTs in the amine-cured epoxy matrix was good, as shown by SEM cross section imaging presented elsewhere [42].

2.2. UV Irradiation

UV irradiation of neat epoxy and MWCNT epoxy nanocomposite films was performed using a NIST-developed 2 m SPHERE [39] as previously described [37]. This SPHERE UV chamber utilizes a mercury arc lamp system that produces a collimated and highly uniform UV flux of approximately 140 W/m^2 in the UVB and UVA (295 nm to 400 nm) range, which is the most detrimental range on polymer degradation. Although the spectrum of this light source contains some radiation having wavelength in the visible range (Figure S2), previous studies [43, 44] on wavelength effect indicated that the degradation of epoxy

caused by radiation > 400 nm is very small (<1 % of UVB region). In addition, previous results from our laboratory have shown similar degradation mechanisms for multiple experimental conditions between epoxy samples degraded in the NIST SPHERE and in the outdoor environment [43]. The stability of this light source during the experiment was evaluated, and it was shown that there was essentially no change in radiation intensity in the 295 nm to 400 nm region after three months of exposure (Figure S2). It can also precisely control the relative humidity (RH) and temperature. In this study, 25 mm × 25 mm specimens were exposed in the SPHERE UV chamber at 50 °C and 75 % RH. Importantly, the choice to run the experiments at 50 °C was made to increase the degradation rate and also because we have observed that the temperature on composite surfaces during summer outdoor exposure often reaches 50 °C or higher even if the ambient temperature in the environment is lower. Specimens were removed at specified UV doses for various characterizations. For assessing the release of MWCNTs, specimens having a surface area of approximately 78.5 cm^2 and a specially-designed sample holder described previously [9] were employed. This holder consisted of a sample chamber, inlet and outlet to supply humid air to the irradiated specimen, and collectors placed at the bottom of the holder to collect any released particles. A cover made of quartz that allows UV radiation transmitted through and irradiated the specimen was used to seal the holder. A humidity sensor was placed inside the sample holder to monitor RH of the exposure environment. Three types of material having a dimension of approximately 5 mm × 5mm were placed on the collector surface: white poly(tetrafluoroethylene) film, highly polished silicon plate, and conductive tape. The surface of all three liners were analyzed after UV irradiation. A picture of the MWCNT-release assessment holder containing a 0.72 % MWCNT epoxy nanocomposite specimen is displayed in Figure S3.

2.3 Characterization of UV-irradiated Nanocomposites

Mass loss, chemical degradation, surface morphological changes, and release of MWCNTs from UV-irradiated specimens were characterized as a function of UV dose. Mass loss was measured using an analytical balance (Mettler Toledo AB265-S, Columbus, OH) having a resolution of 10^{-5} g, and is expressed as: $(M_t - M_o)/M_o \times 100$, where M_t is the specimen mass at irradiation time t, M_o is the specimen mass before irradiation. Chemical degradation was measured with Fourier transform infrared spectroscopy in the attenuated total reflection mode (FTIR-ATR) and X-ray photoelectron spectroscopy (XPS). FTIR-ATR spectra were recorded at a resolution of 4 cm^{-1} using dry air as a purge gas and a spectrometer equipped with a liquid nitrogen-cooled mercury cadmium telluride (MCT) detector. All spectra were the average of 128 scans. The peak height was used to represent the infrared intensity, which is expressed in absorbance, A. All FTIR results were the average of four specimens. XPS measurements were performed on an Axis Ultra DLD spectrophotometer using 150 W (10 mA, 15 kV) monochromatic, Al Kα X-rays with photoelectrons collected along the surface normal at 20 eV pass energy. Photoelectrons were counted at 0.050 eV steps for 500 ms/step and 2 sweeps. XP spectra of the C (1s) region were taken without charge neutralization for detection of MWCNT surface enhancement, and spectra for semi-quantitative elemental analysis were acquired with charge neutralization. Spectral analysis was conducted using CasaXPS with Tougaard backgrounds fitted to each C (1s) region regardless of the conditions the spectra were acquired. Elemental analysis on neutralized spectra also factored

in contributions from O (1s) and N (1s) from the epoxy matrix as well as Na, Ca and Si contaminants, each of which was fitted with a Shirley background. Elemental percentages are based on the peak area corrected with an elemental sensitivity factor of 1.685, 0.78, 0.477, 1.833, 0.278 and 0.328 for the Na (1s), O (1s), N (1s), Ca (2p), C (1s) and Si (2p) regions, respectively, as provided by the manufacturer. Contaminants are not shown in the results; however, Na, Ca, and Si were each < 1 % of the elemental percentages with the exception of the two highest UV doses, which had silicon at 1.8 % and 5.5 %, respectively. Plotted data points are representative of the average of at least 3 measurements at different locations and the error bars represent one standard deviation.

Surface morphological changes were characterized by scanning electron microscopy (SEM), atomic force microscopy (AFM), and electric force microscopy (EFM). The potential for MWCNT release after irradiation for 4865 MJ/m^2 (i.e., 9 months of exposure) was examined by SEM imaging of the surface of all three collector liners. SEM analysis was performed using a Zeiss Supra-55VP Field Emission SEM. A 5 kV acceleration voltage was used for the surface analysis of the nanocomposites and acceleration voltages over 15 kV were applied during cross sectional analysis of the samples prepared by freeze fracture. As mentioned previously [37], the higher acceleration voltage allows for the visualization of MWCNT morphology within the embedded matrix by charge contrast imaging. Detailed procedures for AFM and EFM measurements were described previously [45]. Briefly, the conventional height and phase images were acquired in normal tapping mode using a Veeco Dimension 3100 atomic force microscope while the EFM images were obtained under lift-mode using a conductive AFM probe with an applied bias voltage ranging between −12 V and +12 V.

3. Results and Discussion

3.1. Effects of UV Irradiation on Bulk Material

The mass loss of neat epoxy and 0.72 % and 3.5 % MWCNT epoxy nanocomposite samples as a function of UV dose in the NIST SPHERE was measured (Figure 1). The results for the neat epoxy and 3.5 % MWCNT nanocomposite were presented previously [37] and are included in this figure for comparison. All samples showed a small increase in mass at the lowest UV dosages. This result was likely due to moisture uptake when the samples were transferred from the 45 % RH ambient condition to the 75 % RH of the exposure chamber, causing a greater mass gain than mass loss from nanocomposite degradation.

For all samples, the mass loss increased as the UV dose increased; however, the MWCNT nanocomposite samples consistently had less mass loss than the neat epoxy samples. The rate of mass loss for the two MWCNT epoxy nanocomposites loadings was nearly identical. Since CNTs have been shown to photostabilize polymers by mainly radiation screening [46], this result suggests that the screening of UV radiation by the MWCNTs was not substantially impacted by the MWCNT concentration in the range of 0.7 % to 3.5 %.

3.2. Effects of UV Irradiation on Nanocomposite Surface Chemistry

Figure 2 shows the FTIR-ATR results from the neat epoxy and MWCNT epoxy nanocomposites samples after UV irradiation. We have described the results for the neat epoxy and 3.5 % MWCNT nanocomposite samples previously [37]. Thus, this discussion will focus on comparing the results for the 0.72 % MWCNT nanocomposite sample to the other two samples at two key IR bands: 1508 cm^{-1} (due to benzene ring) of the epoxy structure and 1726 cm^{-1} (attributed to aldehyde/ketone C=O stretching) formed during UV irradiation. Changes in the 1508 cm^{-1} and 1726 cm^{-1} bands represent chain scission and photo-oxidation, respectively. The full difference FTIR-ATR spectra for the 0.72 % MWCNT nanocomposite sample are provided in Figure S4. Both MWCNT nanocomposite samples and the neat epoxy showed rapid degradation under this UV/RH/T environment with a similar decrease of the 1508 cm^{-1} band and increase of the 1726 cm^{-1} band between 0 MJ/m^2 and 166 MJ/m^2. This result suggests that the degradation rate of the matrix surface layer (< 2.5 μm, [37]) in this dose range (i.e., early stage of degradation) was independent of the MWCNT loading. For both MWCNT epoxy nanocomposites, these changes reached a plateau at approximately 166 MJ/m^2 dose, but they continued to advance until 270 MJ/m^2 dose for the neat epoxy. Further, the difference in the level of degradation between the three materials was well separated between 166 MJ/m^2 and 425 MJ/m^2. In this range, the 0.72 % CNT composite exhibited a greater degradation than the 3.5 % composite did, likely due to the stronger shielding effect by the larger amount of CNTs accumulated on the surface of the latter. As described previously [37], the intensity decrease of the band at 1726 cm^{-1} at the highest dose for both MWCNT nanocomposite samples is probably due to the substantial accumulation of MWCNT on the sample surface (as shown by SEM and EFM images in a later section), which would decrease the ATR probing depth in the oxidized epoxy layer. In addition, the rough surface topography of the photodegraded MWCNT nanocomposite samples likely decreased the sample-ATR probe contact (hence intensity) and the band intensity of the epoxy matrix.

XPS analysis was applied to answer two questions: (a) are MWCNTs accumulating on the surface by UV irradiation in low MWCNT loading nanocomposites and (b) how does high intensity UV irradiation at very high doses impact the overall surface oxidation? To answer the first question, we evaluated a stack plot of representative, unneutralized C (1s) spectra at each UV dose, as presented in Figure 3(a). The spectral profiles are composed of two differentially charging regions. The first region is reflective of the positively-charged epoxy region at higher binding energies, which is the only feature in the spectra of the unexposed composite and decreases in binding energy with increasing UV dose. The second region, which only became evident after a sufficient dose of UV radiation (≈ 166 MJ/m^2), is located at a static binding energy of ≈ 284.5 eV and is attributed to the conductive MWCNT mats that formed due to UV-induced removal of the surface epoxy contributions, as has been observed previously [37, 47]. In contrast with previous studies, after the C (1s) regions have reached a MWCNT-like state (dose ≈ 425 MJ/m^2), the XP spectra continued to evolve suggesting that the surface of the nanocomposite continued to be modified. One possibility is that the MWCNTs themselves were increasingly oxidized by the UV radiation.

To understand how increased UV dose impacts surface oxidation, the composite's elemental contributions for the C (1s), N (1s), and O (1s) XP spectral regions measured from neutralized spectra were studied (See Figure 3(b)). Over the course of the 4865 MJ/m^2 UV dose irradiation, the surface carbon concentration decreased while the oxygen and nitrogen contributions increased as clearly indicated by the data for the samples exposed for 4865 MJ/m^2. In the early stage of irradiation, however, there was some variation in the overall trend which can be more easily observed in the inset for the O (1s) plot. At low doses, the O (1s) surface concentration increased until it reached a value of (27.8 ± 0.4) % at ≈ 166 MJ/m^2.

The oxygen content then decreased to (19.3 ± 0.2) % at ≈ 425 MJ/m^2, after which it resumed its increase, albeit at a lower rate. The carbon content followed an inverse trend, first decreasing in percent contributions followed by a switch to increasing at ≈ 166 MJ/m^2, and lastly changing to a decrease at ≈ 425 MJ/m^2. One possible explanation for this behavior is that the outermost surface layer, composed mostly of epoxy, was oxidized as a result of irradiation, raising the surface oxygen content. Once the oxidized epoxy was degraded, the MWCNTs increased in surface concentration, resulting in a corresponding decrease in the oxygen content. This is consistent with the FTIR-ATR observations in Figure 2, which shows an initial gain in C=O functionality at 1726 cm^{-1} followed by a gradual loss in roughly the same doses as observed by XPS. The MWCNTs, which are more resistant to UV-induced oxidation, would subsequently be oxidized at a lower rate.

3.3 Effects of UV Irradiation on Nanocomposite Surface Morphology

The evolution of surface morphology of the 0.72 % MWCNT epoxy nanocomposite with UV irradiation dose is displayed in the SEM images (Figure 4). Very few MWCNTs were visible on the surface of the unexposed sample, but MWCNTs had appeared after 166 MJ/m^2 dose (9 d). The concentration of MWCNTs on the sample surface increased with increasing dose until they mostly covered the surface for all samples exposed to a dose of at least 775 MJ/m^2. At this point, the MWCNTs have formed a dense layer on the nanocomposite surface. This observation is consistent with results from AFM and EFM imaging (Figure 5), which also revealed that the UV-irradiated surface was mostly covered with MWCNTs after irradiation to the same dose. Figure 5 also showed that EFM technique, in particular the EFM phase mode, can provide a stronger contrast of MWCNTs on the surface of nanocomposites than that by the AFM technique. This observation is consistent with a previous study on characterization of single-walled CNTs (SWCNTs) embedded in a polymer matrix [45]. From the microscopic results (Figures 4 and 5) and spectroscopic data (Figures 2 and 3), it is suggested that the increased MWCNT concentration on the nanocomposite surface with increasing UV irradiation dose was a result of the matrix degradation. As the epoxy matrix near the surface underwent photodegradation and was gradually degraded, MWCNTs in the nanocomposite were increasingly exposed on the surface [15, 48]. Overall, the results with the 3.5 % and 0.72 % MWCNT epoxy nanocomposite samples yielded similar results with a thick MWCNT surface layer being formed despite the substantial difference in the MWCNT loading of the initial nanocomposite samples. Similar MWCNT surface accumulation has also been observed for nanocomposites exposing to UV radiation in dry or wet environments [14, 17, 28, 32, 37].

SEM analysis of cross sections was also carried out to investigate the surface topography of the UV-irradiated 0.72 % MWCNT epoxy nanocomposite samples at 4865 MJ/m^2 dose. The SEM images showed the formation of a MWCNT surface layer on the sample (Figure 6). In a previous study, the electrical conductivity of the MWCNT surface layer after UV degradation was found to be five times greater than that of the bulk 3.5 % MWCNT nanocomposite [49]. A roughly similar thickness of the MWCNT surface layer was observed after UV irradiation in this study for two doses: 775 MJ/m^2 (data not shown) and a much higher dose of 4865 MJ/m^2. This finding suggests that the MWCNT surface layer was effectively shielding the epoxy matrix underneath from further degradation, thus limiting growth in the thickness of the MWCNT surface layer. Based on experimental evidence, theory, and simulation, the high electrical conductivity MWCNT surface layer formed by UV irradiation has been postulated as due to a combination of matrix removal and densification of the MWCNT-rich domains in the nanocomposites [49].

It is noted that the substantial amount of MWCNTs formed on the UV irradiated nanocomposite surface observed in this study was from an un-stabilized, model amine-cured epoxy matrix containing aromatic chromophores and electron rich N atoms in the polymer main chains. This epoxy material is known to degrade readily under UV irradiation. For commercial epoxies where UV stabilizers are usually incorporated, the rate of matrix degradation during the early stage of exposure is low and it is expected that little or substantially fewer CNTs would be located on the nanocomposite surface. However, in prolonged exposure (duration depends on concentration and efficacy of the stabilizers) when the amount of UV stabilizers has been substantially decreased or depleted due to both photodegradation and physical leaching, the degradation of the matrix is increased, and it is expected that significant MWCNT would be formed on the nanocomposite surface as observed in this study.

3.4. Mechanisms of Release Resistance of the MWCNT Surface Layer

In addition to measuring the matrix degradation and surface morphological changes, which assessed removal of the epoxy surrounding the MWCNTs, this study also assessed the possibility of MWCNT release caused by the UV irradiation of nanocomposite. This was performed by SEM imaging at high magnification the surfaces of the three liners placed at the bottom of the sample holder (Figure S3) after UV irradiating a 0.72 % MWCNT epoxy nanocomposite specimen having a surface area of 78.5 cm^2 for 4865 MJ/m^2 dose (9-month exposure) using the same SPHERE UV chamber. Despite a thick MWCNT surface layer formed on the nanocomposite surface (Figures 4,5,6), the result showed no evidence of either nanocomposite fragments or individual MWCNT on the collector surfaces. This result is in contrast to those from nanocomposites of the same epoxy matrix containing spherical nanosilica. In experiments on these composites, substantial nanocomposite fragments and individual silica nanoparticles were found on the collector surface after irradiating the same size sample exposed to the same UV source for 775 MJ/m^2 dose [9]. This lack of MWCNT spontaneous release (i.e., without applied mechanical forces) observed in this study is similar to that reported previously for other polymer MWCNT composites exposed to weathering environments [14, 17, 28, 32, 37]. It is also in line with other studies that reported a small release amount but only after subjecting the irradiated samples to high shear

forces [31] or water spraying [17]. Except under very high shear [31], where some free standing MWCNTs were observed, most of the release fragments under severe mechanical stresses contained MWCNTs embedded in, or protruded from, the matrices. Additionally, by the use of a probe in an AFM instrument, our previous study has demonstrated that the UV irradiation-induced MWCNT surface layer is more resistant to scratching than the neat epoxy matrix [37]. In summary, the results of the present study and those from the literature strongly suggest that, in the absence of strong applied mechanical forces, the MWCNTs formed on the surface of polymer nanocomposites after exposure to weathering environments or UV radiation are unlikely to be released. It should be noted that the observation of a lack of spontaneous release of MWCNTs after UV irradiation of nanocomposites was studied for only a high aspect ratio MWCNT in a model, unstabilized thermoset epoxy matrix that has a good adhesion with this carbon nanofiller and is known susceptible to degradation by the weathering environments. Additional research is needed on the potential release of MWCNTs having low aspect ratios in more hydrophobic thermoplastic matrices, such as polyolefins, to provide essential data for a more complete assessment of the release of MWCNTs from nanocomposites exposed to UV radiation or weathering conditions. Further investigation is also needed on the effects of mechanical stresses, such as abrasion, and environmental stresses such as free-thaw cycles or hail storms, on the potential rerelease of MWCNTs during UV irradiation or weathering of nanocomposites. Nevertheless, given the lack of evidence of spontaneous release (no applied external stresses) after irradiating to a very high dose of UV radiation or for a long time at high UV intensity, we propose the following plausible mechanisms to explain the strong release resistance of individual MWCNT from the UV- or weather-induced MWCNT surface layer.

3.4.1. Embedded CNTs in Matrix—This mechanism is illustrated in Figure 7a. Although increasing amounts of MWCNTs are exposed on the surface as the matrix is degraded by UV irradiation, parts of some protruding MWCNTs are still embedded (anchored) in the matrix. Due to their strong adhesion with most polymers, the embedded MWCNTs are not likely to leave the nanocomposite surface without breaking the matrix. The strong MWCNT-polymer adhesion is due to the similarity of surface free energies between these two materials. MWCNTs have a surface free energy (γ^s) of approximately 45.3 mJ/m^2 [50], which is similar to that of amine-cured epoxy (46.2 mJ/m^2) [51] and higher than that of most common polymers [52]. A filler will be readily wetted (low contact angle) by a matrix when the surface energy of the filler is similar to or higher than that of the matrix resin. Therefore, MWCNTs should form strong bonds with most polymers [50, 53]. For the bisphenol A-based epoxy matrix used in this study, the adhesion is enhanced by the π-π interactions between the MWCNT surfaces and the aromatic units in the epoxy resin [54, 55]. Such interactions have been found to result in approximately 30 % and 44 % higher interfacial fracture energy and bonding strength (pull-off), respectively, between MWCNTs and epoxy than those between MWCNTs and non-aromatic polymers [55].

3.4.2. CNT Entanglements—Another reason for the strong release resistance of the MWCNT surface layer is attributed to their entanglement characteristics. As seen in Figure 4, the MWCNT surface layer appears as a dense, entangled network. Similar entangled

networks have been observed for MWCNT accumulation on the sample surface of other MWCNT polymer nanocomposites exposed to weathering environments [14, 17, 28, 31, 37]. The entangled MWCNT network formation is not unique to the surface layer formed by the UV irradiation of nanocomposites, but is generally observed in polymer nanocomposites made of both SWCNTs and MWCNT, even at low loadings [56, 57]. The main driving force for CNT entanglements is their large aspect ratio and the van der Waals interactions between different parts of the CNTs. That is, when the two ends of a CNT that has a length greater than a critical length get closer, they will join to each other under the driving force of van der Waals interactions, and a racket-like, folded CNT is formed [58]. Entanglement is one of the main mechanisms responsible for the increase of load transfer in polymer CNT composites [58], and has been modeled by different methods [57, 58]. We believe this CNT entanglement provides a strong mechanical hooking that prevents individual MWCNT from leaving the MWCNT surface layer, even under applied mild mechanical stress such as sonication. In particular, the entanglement is likely an important mechanism to preventing some protruded MWCNTs that are no longer embedded in the matrix from releasing because they still interweave with the embedded ones.

3.4.3. Matrix-CNT Bonding in the MWCNT Surface Layer—Another reason that can also contribute to the release resistance of the UV-induced MWCNT surface layer is the bonding between the MWCNTs and the partially-degraded matrix in this layer. This is illustrated in Figure 7b, which shows some MWCNTs or their bundles in the entangled MWCNT surface layer are still bonded together by residual or partially-degraded matrix material. For samples with MWCNTs well dispersed in the polymer matrix, which is the case for this study, previous work [42] has shown that each MWCNT or each small MWCNT bundle is completely covered by the matrix. As the matrix is degraded and the MWCNT surface layer is formed by irradiation, it is expected that, depending on the UV dose level, parts of some tubes or their bundles in this layer are still covered with the matrix material, particularly for areas that are not directly exposed to the radiation. This matrix material can provide a strong bonding between two or more MWCNTs and their bundles, and can effectively reduce their possibility for release.

3.4.4. van der Waals Interactions between MWCNT—The van der Waals interactions between the MWCNT can also potentially prevent them from leaving the surface layer formed during UV irradiation or weathering. The van der Waals interaction between two carbon nanotubes has been measured to be ≈ 500 eV/μm [59]. This strong interaction between CNTs is the main reason for their tendency to aggregate with each other and the need for application of high energy mixing to disperse them in polymeric materials. When the matrix in the MWCNT surface layer is completely removed by UV radiation or weathering environments, the matrix-free MWCNTs would likely still stick together because of their strong van der Waals interactions. Although such an interaction is weaker than that between the MWCNTs and the polymer matrix, binding between the protruded, matrix-embedded MWCNTs and protruded, non-embedded MWCNTs can potentially inhibit the latter from releasing from the MWCNT surface layer.

These mechanisms for the release resistance of the MWCNTs formed on the nanocomposite surface subject to UV irradiation are proposed based solely on known material properties of the MWCNT and its interaction with an amine-cured epoxy. Experimental data are needed using very short MWCNTs so that the entanglement phenomenon is eliminated and the extent of van der Waals force interactions between CNTs is substantially reduced in both amine-cured epoxy and hydrophobic polyethylene matrices to verify some of these proposed mechanisms.

4. Conclusions

This study has investigated the degradation of a 0.72 % MWCNT/amine-cured epoxy nanocomposite exposed to UV radiation at various doses, the effects of these UV exposures on the surface accumulation and release of MWCNTs, and possible mechanisms responsible for the strong release resistance of the MWCNT surface layer formed on nanocomposites by UV irradiation. Irradiated samples were characterized for chemical degradation, mass loss, surface morphological changes, and MWCNT release using a variety of analytical techniques. The results showed that, under UV radiation, the epoxy matrix underwent photodegradation that produced an accumulation of MWCNTs on the surface. The MWCNT aggregated and formed a dense, entangled network structure that decreased the degradation of the epoxy polymer layer underneath, an identical finding to that obtained after UV irradiation of the 3.5 % MWCNT epoxy nanocomposite samples. This also reduced the MWCNT surface layer growth with increasing UV dose. No evidence of MWCNT release was observed during UV irradiation, even at a very high dose (4865 MJ/m^2, equivalent to 9-month exposure). We believe such strong resistance to release of the MWCNT surface layer formed by UV irradiation of polymer nanocomposites is due to four main mechanisms: 1) part of the surface-exposed MWCNTs are still embedded in the polymer matrix, 2) the entanglement propensity of CNTs, which mechanically hook matrix-free MWCNTs with matrix-embedded MWCNT, 3) surface-exposed MWCNTs are still bonded together by partially-degraded matrix, and 4) strong van der Waals interactions between matrix-free MWCNTs. Additional research is needed to investigate the relative impact of these four different mechanisms for different types of MWCNT polymer nanocomposites and MWCNT loadings and how these mechanisms would influence the potential for CNT release after additional environmental and mechanical stresses. Understanding the processes that cause the formation of the MWCNT surface layer and the underlying reasons that hinder or facilitate the release of MWCNTs from polymer nanocomposites exposed to weathering elements can play a critical role in the design of safe, sustainable nanocomposites for applications in various industries.

Acknowledgments

Research performed in part at the NIST Center for Nanoscale Science and Technology.

References

1. Wohlleben W, Neubauer N. Quantitative rates of release from weathered nanocomposites are determined across 5 orders of magnitude by the matrix, modulated by the embedded nanomaterial. Nano Impact. 2016; 1:39–45.

2. Chinnappan A, Baskar C, Kim H, Ramakrishna S. Carbon nanotube hybrid nanostructures: future generation conducting materials. J Mater Chem A. 2016; 4(24):9347–9361.
3. Zhang J, Terrones M, Park CR, Mukherjee R, Monthioux M, Koratkar N, et al. Carbon science in 2016: Status, challenges and perspectives. Carbon. 2016; 98:708–732.
4. Liu YY, Zhao J, Zhao LY, Li WW, Zhang H, Yu X, et al. High Performance Shape Memory Epoxy/ Carbon Nanotube Nanocomposites. ACS Appl Mater Interf. 2016; 8(1):311–320.
5. Nadiv R, Shtein M, Refaeli M, Peled A, Regev O. The critical role of nanotube shape in cement composites. Cem Concr Compos. 2016; 71:166–174.
6. Nowack B, David RM, Fissan H, Morris H, Shatkin JA, Stintz M, et al. Potential release scenarios for carbon nanotubes used in composites. Environ Intl. 2013; 59(0):1–11.
7. Petersen EJ, Zhang LW, Mattison NT, O'Carroll DM, Whelton AJ, Uddin N, et al. Potential release pathways, environmental fate, and ecological risks of carbon nanotubes. Environ Sci Technol. 2011; 45(23):9837–9856. [PubMed: 21988187]
8. Gorham JM, Nguyen T, Bernard C, Stanley D, Holbrook RD. Photo-induced surface transformations of silica nanocomposites. Surf Interface Anal. 2012; 44(13):1572–1581.
9. Nguyen T, Pellegrin B, Bernard C, Rabb S, Stuztman P, Gorham JM, et al. Characterization of Surface Accumulation and Release of Nanosilica During Irradiation of Polymer Nanocomposites by Ultraviolet Light. J Nanosci Nanotechnol. 2012; 12(8):6202–6215. [PubMed: 22962727]
10. Gottschalk F, Nowack B. The release of engineered nanomaterials to the environment. J Environ Monit. 2011; 13(5):1145–1155. [PubMed: 21387066]
11. Asmatulu R, Mahmud GA, Hille C, Misak HE. Effects of UV degradation on surface hydrophobicity, crack, and thickness of MWCNT-based nanocomposite coatings. Progress in Organic Coatings. 2011; 72(3):553–561.
12. Wohlleben W, Vilar G, Fernandez-Rosas E, Gonzalez-Galvez D, Gabriel C, Hirth S, et al. A pilot interlaboratory comparison of protocols that simulate aging of nanocomposites and detect released fragments. Environ Chem. 2014; 11(4):402–418.
13. Froggett SJ, Clancy SF, Boverhof DR, Canady RA. A review and perspective of existing research on the release of nanomaterials from solid nanocomposites. Part Fibre Toxicol. 2014; 11
14. Ging J, Tejerina-Anton R, Ramakrishnan G, Nielsen M, Murphy K, Gorham JM, et al. Development of a conceptual framework for evaluation of nanomaterials release from nanocomposites: Environmental and toxicological implications. Sci Tot Environ. 2014; 473:9–19.
15. Duncan TV. Release of Engineered Nanomaterials from Polymer Nanocomposites: the Effect of Matrix Degradation. ACS Appl Mater Interf. 2015; 7(1):20–39.
16. Schlagenhauf L, Nüesch F, Wang J. Release of Carbon Nanotubes from Polymer Nanocomposites. Fibers. 2014; 2(2):108.
17. Fernández-Rosas E, Vilar G, Janer G, González-Gálvez D, Puntes V, Jamier V, et al. Influence of nanomaterials compatibilization strategies in polyamide nanocomposite properties and nanomaterials release during the use phase. Environ Sci Technol. 2016; 50(5):2584–2594. [PubMed: 26830469]
18. Reed RB, Goodwin DG, Marsh KL, Capracotta SS, Higgins CP, Fairbrother DH, et al. Detection of single walled carbon nanotubes by monitoring embedded metals. Environ Sci Proc Imp. 2013; 15(1):204–213.
19. Petersen EJ, Diamond SA, Kennedy AJ, Goss GG, Ho K, Lead J, et al. Adapting OECD Aquatic Toxicity Tests for Use with Manufactured Nanomaterials: Key Issues and Consensus Recommendations. Environ Sci Technol. 2015; 49(16):9532–9547. [PubMed: 26182079]
20. Edgington AJ, Petersen EJ, Herzing AA, Podila R, Rao A, Klaine SJ. Microscopic investigation of single-wall carbon nanotube uptake by Daphnia magna. Nanotoxicology. 2014; 8(S1):2–10. [PubMed: 24350828]
21. Godwin H, Nameth C, Avery D, Bergeson LL, Bernard D, Beryt E, et al. Nanomaterial Categorization for Assessing Risk Potential To Facilitate Regulatory Decision-Making. ACS Nano. 2015; 9(4):3409–3417. [PubMed: 25791861]
22. Aschberger K, Johnston HJ, Stone V, Aitken RJ, Hankin SM, Peters SAK, et al. Review of carbon nanotubes toxicity and exposure-Appraisal of human health risk assessment based on open literature. Crit Rev Toxicol. 2010; 40(9):759–790. [PubMed: 20860524]

23. Schlagenhauf L, Kianfar B, Buerki-Thurnherr T, Kuo YY, Wichser A, Nuesch F, et al. Weathering of a carbon nanotube/epoxy nanocomposite under UV light and in water bath: impact on abraded particles. Nanoscale. 2015; 7(44):18524–18536. [PubMed: 26490158]
24. Selck H, Handy RD, Fernandes TF, Klaine SJ, Petersen EJ. Nanomaterials in the aquatic environment: A European Union–United States perspective on the status of ecotoxicity testing, research priorities, and challenges ahead. Environ Toxicol Chem. 2016; 35(5):1055–1067. [PubMed: 27089437]
25. Bello D, Wardle BL, Yamamoto N, deVilloria RG, Garcia EJ, Hart AJ, et al. Exposure to nanoscale particles and fibers during machining of hybrid advanced composites containing carbon nanotubes. J Nano Res. 2009; 11(1):231–249.
26. Bello D, Wardle BL, Zhang J, Yamamoto N, Santeufemio C, Hallock M, et al. Characterization of Exposures To Nanoscale Particles and Fibers During Solid Core Drilling of Hybrid Carbon Nanotube Advanced Composites. Int J Occ Saf Environ Health. 2010; 16(4):434–450.
27. Cena LG, Peters TM. Characterization and control of airborne particles emitted during production of epoxy/carbon nanotube nanocomposites. J Occ Environ Hyg. 2011; 8(2):86–92.
28. Wohlleben W, Brill S, Meier MW, Mertler M, Cox G, Hirth S, et al. On the Lifecycle of Nanocomposites: Comparing Released Fragments and their In-Vivo Hazards from Three Release Mechanisms and Four Nanocomposites. Small. 2011; 7(16):2384–2395. [PubMed: 21671434]
29. Huang GN, Park JH, Cena LG, Shelton BL, Peters TM. Evaluation of airborne particle emissions from commercial products containing carbon nanotubes. J Nano Res. 2012; 14(11)
30. Schlagenhauf L, Chu BTT, Buha J, Nuesch F, Wang J. Release of Carbon Nanotubes from an Epoxy-Based Nanocomposite during an Abrasion Process. Environ Sci Technol. 2012; 46(13): 7366–7372. [PubMed: 22662874]
31. Hirth S, Cena L, Cox G, Tomović Ž, Peters T, Wohlleben W. Scenarios and methods that induce protruding or released CNTs after degradation of nanocomposite materials. J Nano Res. 2013; 15(4):1–15.
32. Wohlleben W, Meier MW, Vogel S, Landsiedel R, Cox G, Hirth S, et al. Elastic CNT–polyurethane nanocomposite: synthesis, performance and assessment of fragments released during use. Nanoscale. 2013; 5(1):369–380. [PubMed: 23172121]
33. Schlagenhauf L, Buerki-Thurnherr T, Kuo YY, Wichser A, Nuesch F, Wick P, et al. Carbon Nanotubes Released from an Epoxy-Based Nanocomposite: Quantification and Particle Toxicity. Environ Sci Technol. 2015; 49(17):10616–10623. [PubMed: 26251010]
34. Boonruksa P, Bello D, Zhang JD, Isaacs JA, Mead JL, Woskie SR. Characterization of Potential Exposures to Nanoparticles and Fibers during Manufacturing and Recycling of Carbon Nanotube Reinforced Polypropylene Composites. Ann Occup Hyg. 2016; 60(1):40–55. [PubMed: 26447230]
35. Wohlleben W, Meyer J, Muller J, Muller P, Vilsmeier K, Stahlmecke B, et al. Release from nanomaterials during their use phase: combined mechanical and chemical stresses applied to simple and multi-filler nanocomposites mimicking wear of nano-reinforced tires. Environmental Science-Nano. 2016; 3(5):1036–1051.
36. Wohlleben W, Kingston C, Carter J, Sahle-Demessie E, Vázquez-Campos S, Acrey B, et al. NanoRelease: Pilot interlaboratory comparison of a weathering protocol applied to resilient and labile polymers with and without embedded carbon nanotubes. Carbon. 2017; 113:346–360.
37. Petersen EJ, Lam T, Gorham JM, Scott KC, Long CJ, Stanley D, et al. Methods to assess the impact of UV irradiation on the surface chemistry and structure of multiwall carbon nanotube epoxy nanocomposites. Carbon. 2014; 69:194–205.
38. Kamal, M., Huang, B. Natural and Artificial Weathering of Polymers. In: Hamid, S.Amin, M., Maadhah, A., editors. Handbook of Polymer Degradation. Marcel Dekker; New York: 1992. p. 127-178.
39. Chin J, Byrd E, Embree N, Garver J, Dickens B, Finn T, et al. Accelerated UV weathering device based on integrating sphere technology. Rev Sci Instrum. 2004; 75(11):4951–4959.
40. Singh D, Sotiriou GA, Zhang F, Mead J, Bello D, Wohlleben W, et al. End-of-life thermal decomposition of nano-enabled polymers: effect of nanofiller loading and polymer matrix on by-products. Environ Sci: Nano. 2016

41. O'Carroll DM, Liu X, Mattison NT, Petersen EJ. Impact of diameter on carbon nanotube transport in sand. J Coll Interf Sci. 2013; 390:96–104.
42. Banerjee D, Nguyen T, Chuang TJ. Mechanical properties of single-walled carbon nanotube reinforced polymer composites with varied interphase's modulus and thickness: A finite element analysis study. Computational Materials Science. 2016; 114:209–218.
43. Gu, X., Dickens, B., Stanley, D., Byrd, WE., Nguyen, T., Vaca-Trigo, I., et al. Linking Accelerating Laboratory Test with Outdoor Performance Results for a Model Epoxy Coating System. In: Martin, JW.Ryntz, RA.Chin, J., Dickie, RA., editors. Service Life Prediction of Polymeric Materials. Springer; New York: 2008.
44. Vaca-Trigo, I., Meeker, WQ. A Statistical model for linking field and laboratory exposure results for a model coating. In: Martin, JW.Ryntz, RA.Chin, J., Dickie, RA., editors. Service Life Prediction of Polymeric Materials. Springer; New York: 2008.
45. Zhao M, Gu X, Lowther SE, Park C, Jean YC, Nguyen T. Subsurface characterization of carbon nanotubes in polymer composites via quantitative electric force microscopy. Nanotechnol. 2010; 21(22):225702.
46. Najafi E, Shin K. Radiation resistant polymer-carbon nanotube nanocomposite thin films. Colloids Surf, A. 2005; 257–58:333–337.
47. Gorham JM, Woodcock JW, Scott KC. NIST SP 1200-10: Challenges, Strategies and Opportunities for Measuring Carbon Nanotubes within a Polymer Composite by X-ray Photoelectron Spectroscopy. 2015:13.
48. Nguyen, T., Wohlleben, W., Sung, LP. Mechanisms of Aging and Release from Weathered Nanocomposites. Vol. Chap. 14. Taylor & Francis; Boca Raton, FL: 2014.
49. Long CJ, Orloff ND, Twedt KA, Lam T, Vargas-Lara F, Zhao M, et al. Giant surface conductivity enhancement in a carbon nanotube composite by ultraviolet light exposure. ACS Appl Mater Interf. 2016; 8(35):23230–23235.
50. Nuriel S, Liu L, Barber AH, Wagner HD. Direct measurement of multiwall nanotube surface tension. Chem Phys Let. 2005; 404(4–6):263–266.
51. Kinloch, AJ., editor. Durability of Structural Adhesives. Applied Science; N.Y: 1983. p. 10
52. Wu, S. Polymer Interface and Adhesion. Marcel Dekker, Inc; New York: 1982. p. 169-180.
53. Wagner HD, Vaia RA. Nanocomposites: issues at the interface. Materials Today. 2004; 7(11):38–42.
54. Yang MJ, Koutsos V, Zaiser M. Interactions between polymers and carbon nanotubes: A molecular dynamics study. J Phys Chem B. 2005; 109(20):10009–10014. [PubMed: 16852210]
55. Chen X, Zhang L, Zheng M, Park C, Wang X, Ke C. Quantitative nanomechanical characterization of the van der Waals interfaces between carbon nanotubes and epoxy. Carbon. 2015; 82:214–228.
56. Zhao M, Ming B, Kim J-W, Gibbons LJ, Gu X, Nguyen T, et al. New insights into subsurface imaging of carbon nanotubes in polymer composites via scanning electron microscopy. Nanotechnol. 2015; 26(8)
57. Vargas-Lara F, Douglas JF. Confronting the complexity of CNT materials. Soft Matter. 2015; 11(24):4888–4898. [PubMed: 26008627]
58. Lu W, Chou TW. Analysis of the entanglements in carbon nanotube fibers using a self-folded nanotube model. Journal of the Mechanics and Physics of Solids. 2011; 59(3):511–524.
59. Girifalco LA, Hodak M, Lee RS. Carbon nanotubes, buckyballs, ropes, and a universal graphitic potential. Phys Rev B: Condens Matter. 2000; 62(19):13104–13110.

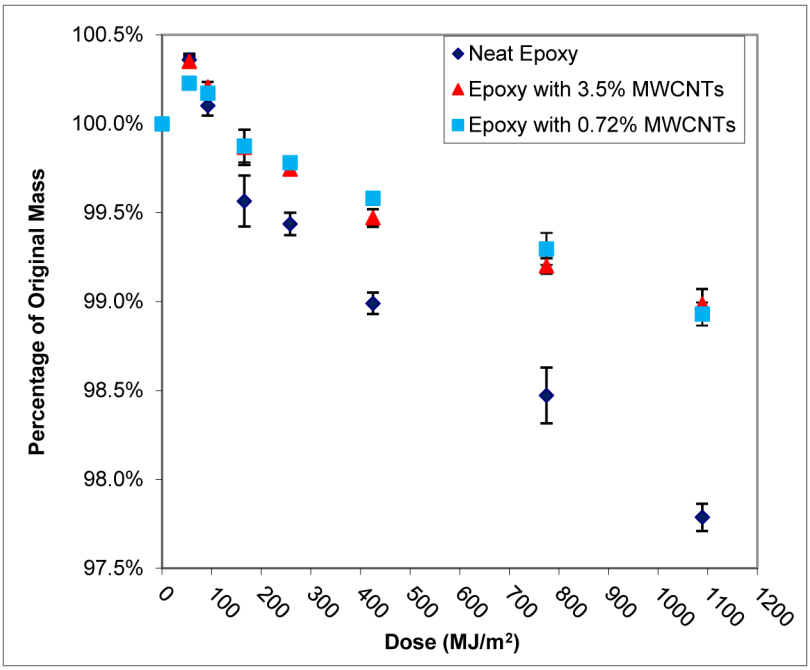

Figure 1.

Remaining mass as a function of dose for neat epoxy, 0.72 % MWCNT epoxy nanocomposite samples, and 3.5 % MWCNT epoxy nanocomposite samples exposed to UV radiation at 50 °C and 75 % relative humidity. Data for the neat epoxy and 3.5 % MWCNT epoxy nanocomposite samples is taken from Reference 37 with permission from Carbon. Results are the average of five specimens (except for the 775 MJ/m^2 and 1089 MJ/m^2 samples for the neat epoxy for which n=4), and error bars represent one standard deviation.

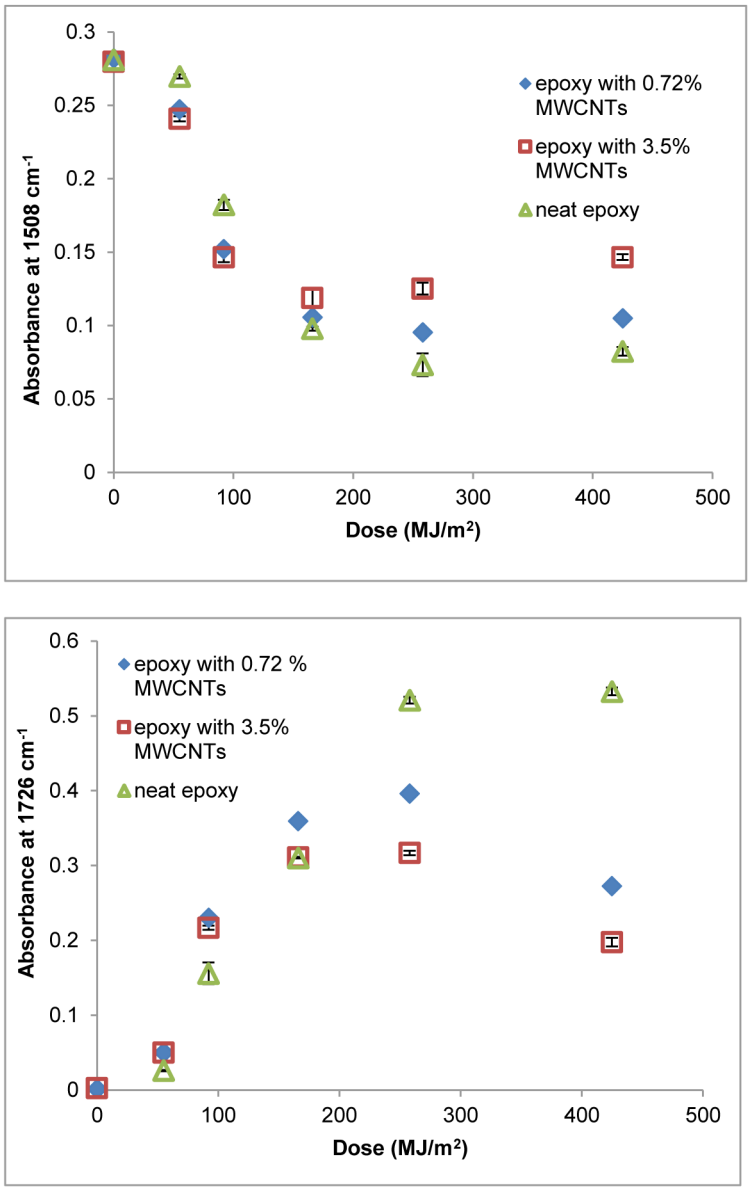

Figure 2.

Changes in FTIR-ATR intensity for (upper) 1508 cm^{-1} and (lower) 1726 cm^{-1} bands for neat epoxy, 0.72 % MWCNT epoxy nanocomposite samples, and 3.5% MWCNT epoxy nanocomposite samples before and after UV irradiation with varying doses. Data for the neat epoxy and 3.5 % MWCNT epoxy nanocomposite samples is taken from Reference 37 with permission from Carbon. Each data point was the average of three specimens, and the error bars represent one standard deviation.

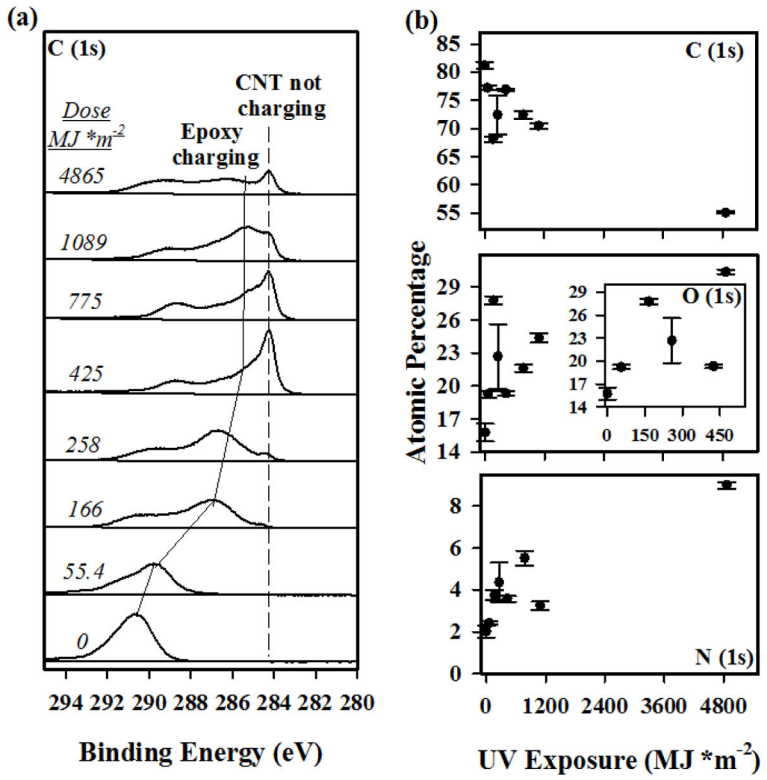

Figure 3.

(a) Representative C(1s) spectra at different UV doses acquired in the absence of charge neutralization for the 0.72 % MWCNT epoxy nanocomposite samples. Electron vacancies lead to unfilled, positively charged orbitals resulting in a surface characterized by a peak shifted to higher binding energies (epoxy charging) and the conductive MWCNTs begin to surface accumulate around 166 MJ/m^2. (b) Elemental analysis of the 3 dominant elements from separate XP spectra acquired under charge neutralization. The O (1s) region has an inset representative of the first 500 MJ/m^2. Plotted data points are representative of the average of at least 3 measurements at different locations and the error bar represent one standard deviation.

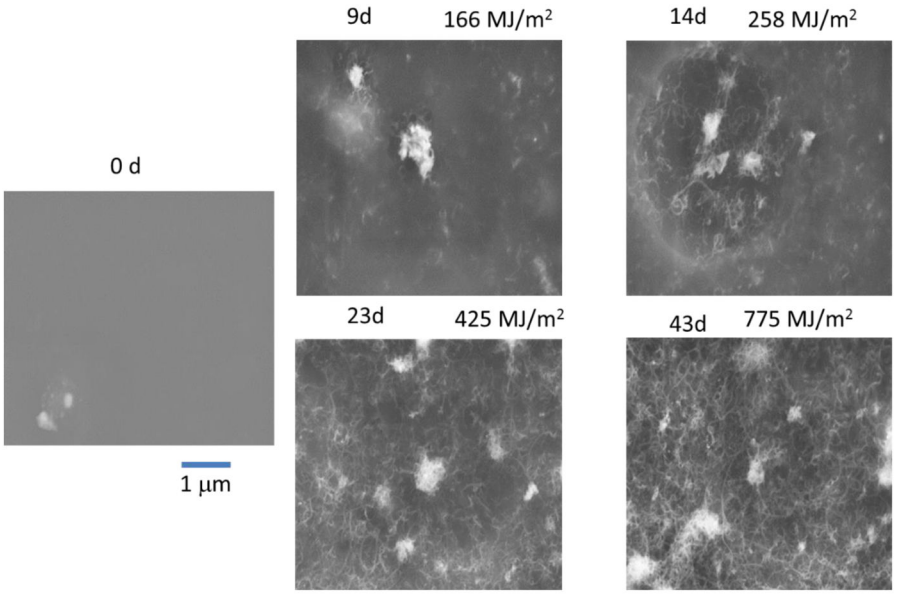

Figure 4.

SEM images of 0.72 % MWCNT epoxy nanocomposite before and after UV irradiation at various doses. The scale bar is 1 μm.

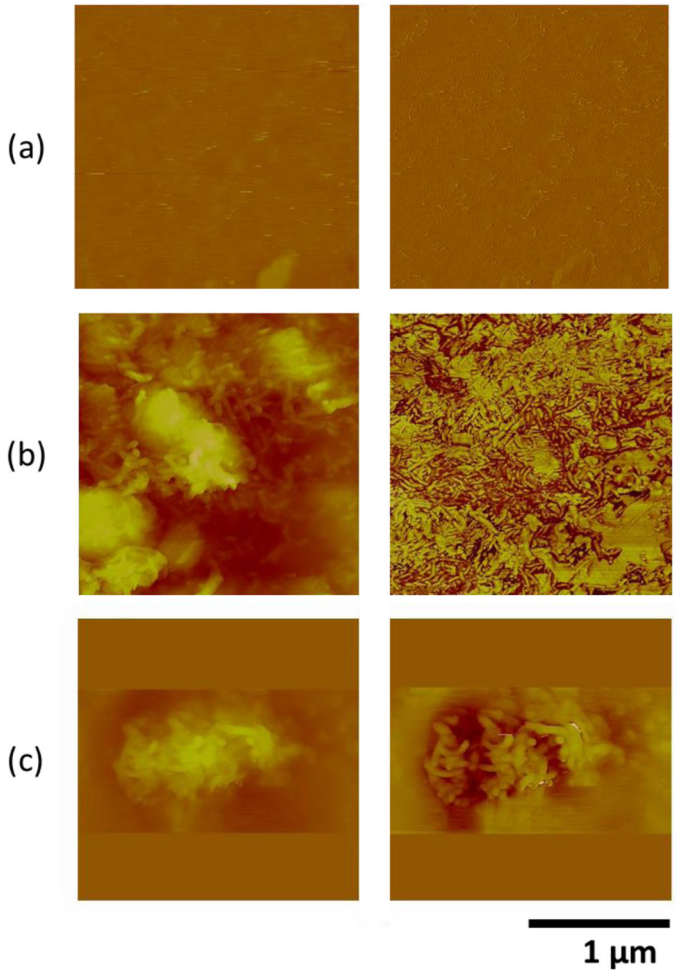

Figure 5.

AFM and EFM height and phase images of 0.72 % MWCNT epoxy nanocomposite surface before and after UV irradiation; a): AFM images before irradiation, b) AFM images after irradiation at 775 MJ/m^2 dose, and c) EFM images after irradiation at 775 MJ/m^2. Scan size is 2 μm. For each pair, height image is on the left and phase image is on the right. The height range of the image is roughly from 0 nm to 800 nm.

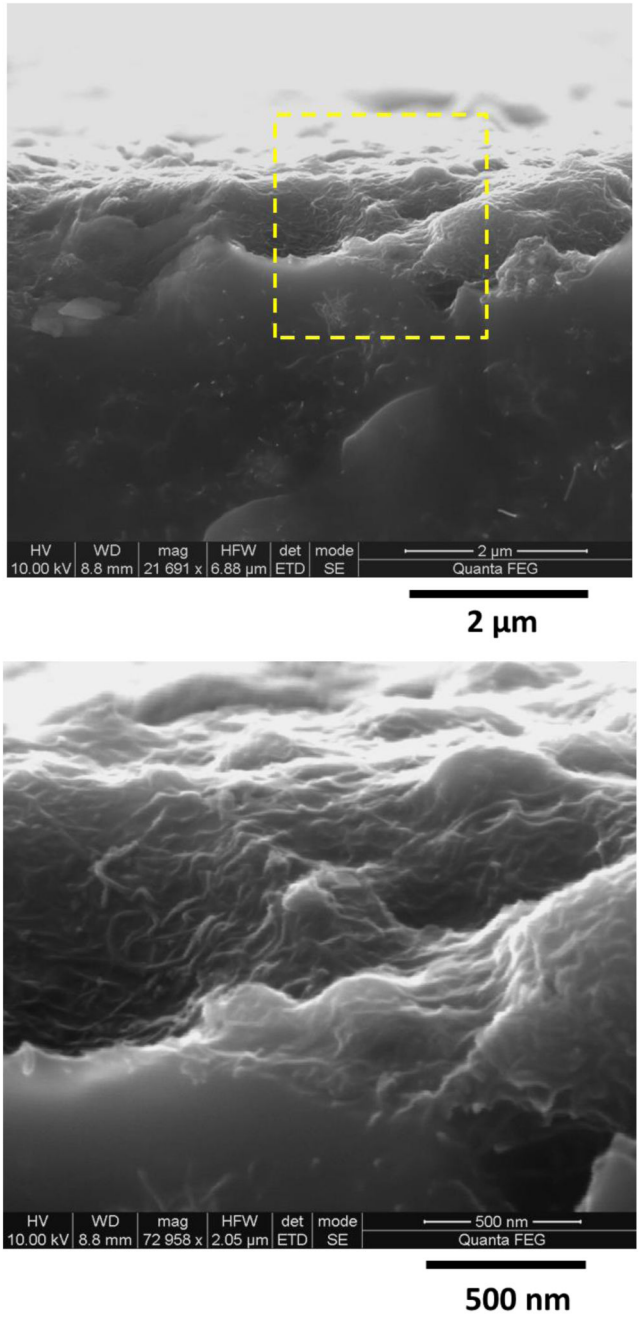

Figure 6.

SEM cross section images after 4865 MJ/m^2 dose (top) and at high magnification(bottom) for the 0.72 % MWCNT epoxy nanocomposite samples.

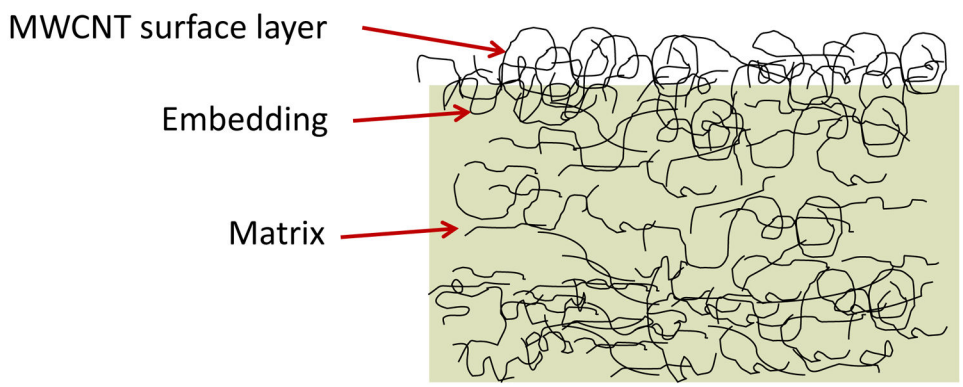

Figure 7a

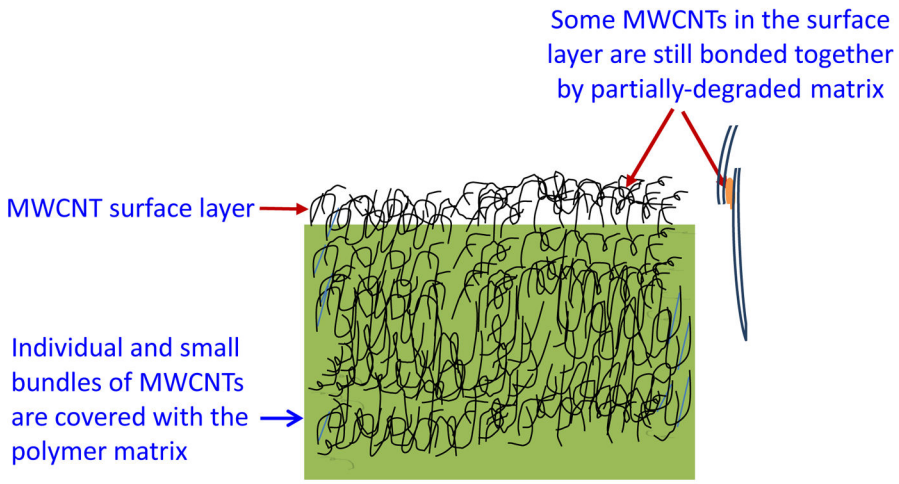

Figure 7b

Figure 7.

Schematic figures showing two of the four likely mechanisms responsible for the release resistance of UV-induced MWCNT surface layer; a) matrix-embedded MWCNT, and b) MWCNT are bonded by partially-degraded matrix.